Journal of Ceramic Processing Research. Vol. 25, No. 2, pp. 234~241 (2024)
(Received 6 December 2023, Received in revised form 9 February 2024, Accepted 15 February 2024)
https://doi.org/10.36410/jcpr.2024.25.2.234

J O U R N A L O F
Ceramic Processing Research

Comparison of WC and SiO_2 mill additives for abrasion resistance sodium borosilicate glass-ceramics coating

Yasin Bozkurt Yılmaz[a,b,*], Oğuz Karaahmet[a,b] and Buğra Çiçek[a]
[a]*Yıldız Technical University, Department of Metallurgy and Materials Science Engineering, 34210 Esenler/Istanbul/Türkiye*
[b]*Akcoat R&D Center, 2nd IZ, 54300 Hendek/Sakarya/Türkiye*

Vitreous enamel (glass-ceramic) coatings are used to improve surface properties of metals due to their chemical and high temperature resistance. With the widespread use of enamelled products, it is necessary to develop enamels with high abrasion resistance, which protects their performance in abrasive environment such as scratches and friction damage. In this study, tungsten carbide (WC) and quartz (SiO_2) were added as mill additives into the enamel composition in proportions ranging from 0 wt.% to 8 wt.%. An XRD analysis was performed to examine the effects of additives on crystal phases. Depending on the additive type, SiO_2, $CaWO_4$ and WC phases were observed. The batches were applied on cast iron. The abrasion resistance of the enamelled cast iron surfaces were investigated by PEI test (ISO 10545-7). An SEM-EDS analysis were carried out to investigate the fracture mechanism and the effects of addition on the microstructure. The analyses reveal that surface morphology and abrasion resistance of the enamel coatings change depending on the mill additive rate. With 8 wt.% WC and 8 wt.% SiO_2 addition, the abrasion resistance was improved by 51.80% compared to the standard sample.

Keywords: Enamel, Glass ceramics, Abrasion resistance, Additive, Surface properties.

Introduction

Vitreous enamels (glass-ceramic coatings), also known as porcelain enamels, are inorganic coating materials used to improve the surface properties of metals [1]. Glass-ceramics are structures obtained by controlled crystallisation in the glassy phase and have superior properties due to their composite structure [2]. Glass-ceramic coatings improve the chemical and high-temperature resistance of the metal on which they are coated, increase the corrosion resistance and facilitate the desired aesthetic appearance including, for example, color, lustre and opacity [3]. Vitreous enamel coatings are used in widespread fields of industry where physical and chemical resistance is required, i. e. kitchen equipments, heat exchangers and boilers [4-7].

Frit (a glass ceramic structured raw material) and mill additives form the coating composition [8, 9]. Frit consists of various oxides obtained by high-temperature melting (1100-1450 °C) and subsequent cooling of multiple raw materials, such as quartz (SiO_2), feldspar ($MAl_xSi_yO_z$) sodium borate ($Na_2[B_4O_5(OH)_5]\cdot 8H_2O$) and carbonate ($MCO_3^{-2}$). Mill additives are used to provide properties such as refractoriness, color and gloss values, chemical resistance, which cannot be obtained during the production of glass-ceramics and which are desired to be improved [1, 10]. In glass-ceramic coatings, mill additives are ground together with the frit at the stage of final product production before application. They are obtained from minerals such as clay, quartz and feldspar, or can be synthetic, such as pigment and nitrate. Enamel coatings are generally applied by two basic methods: dry and wet coating. Mill additives vary depending on the enamel coating method and regulate the application parameters as well as the enamel properties on the metal surface [11, 12].

Mechanical abrasions, such as scratches and friction damage the enamel surface; hence, enamel loses the ability to protect the ground metal. When enamels are used in cookware and boilers, enamel-coated surfaces undergo mechanical, chemical and thermal abrasion. In particularly, the removal of coating from the cookware surface leads to the metal ion transfer from the substrate metal into the food. These metal ions migrate to the human body through food and are stored in the body. Studies have shown that metal ions (e.g., Al, Ni) migrating into the body can cause serious illnesses [13, 14]. Therefore, enhancing the coating's abrasion resistance is imperative, as it plays a paramount role in safeguarding human health.

The first studies aimed at improving the abrasion resistance of the coating were related to the enamel structure. In studies with different enamel compositions to apply on low carbon steel surface, it was observed that the abrasion resistance of the enamel having a closed porosity structure was lower [15]. In another study, it

*Corresponding author:
Tel : +90 264 323 30 31
Fax: +90 264 323 30 32
E-mail: yasin.yilmaz@akcoat.com

was observed that the abrasion resistance of the enamels having good acid resistance was better than the enamels having weak acid resistance. In addition, tin oxide (SnO_2) mill additive to 1% was found to improve abrasion resistance [16]. In recent studies, mill additives have been used to improve the mechanical properties of enamels. In the experiments with 30 wt.% potassium feldspar ($KAlSi_3O_8$) and 30 wt.% zirconium silicate ($ZrSiO_4$) mill additives, it was seen that the surface defects started to appear, and the abrasion resistance get worse [17]. In another study, the effect of using zircon, spodumene, feldspar, and quartz as an additive was examined, and it was observed that the use of feldspar, zircon, and high amount of spodumene had a negative effect on abrasion resistance. The 10 wt.% quartz addition has been shown to improve mechanical properties without loss of other properties [11]. In the study conducted on aluminum enamel, the effect of spodumene, quartz, WC, SiC and graphite mill additive on abrasion resistance was investigated. It has been observed that 10% spodumene or quartz additive improves abrasion resistance and graphite additive causes flake formation and decrease abrasion resistance. In addition, agglomerated particles were found to increase the porosity in the structure [18]. Rossi et al., aluminum was preferred as metallic base in the study [18]. Aluminum enamels (T_f < 570 °C) are fired at low temperature compared to cast iron enamels (T_f < 750 °C) and low carbon steel enamels (T_f > 820 °C). For this reason, the reactions that will take place during firing are different. In addition, the reactions and phase transformations of WC and WO_3 with enamel oxides are not studied.

In these studies, generally the effects of hard ceramic particles on the surface properties and mechanical strength of the coating were examined. There are no publications researching the reactions and phase transformations of additives with the glass-ceramic structure. In this paper, we investigate the effects of only wolfram carbide (WC), only quartz (SiO_2) and quartz combined WC (WC + SiO_2) mill additives on the surface morphology and abrasion resistance of cast iron enamel coatings. WC is preferred as an additive to increase the abrasion resistant materials due to its high hardness (HV=26 GPa) [19, 20]. SiO_2 has been used due to its refractory character and network former properties [1]. In addition, since SiO_2 acts as a network former, it ensures compatibility between WC and the glass-ceramic structure. The prepared enamel batches were applied by wet spray on cast iron. Surface properties were analysed by spectrophotometer and optical microscope. An XRD analysis was performed to determine the enamel phases. The effects of mill additives on enamel abrasion resistance was investigated by a PEI (ISO 10545-7). The abrasion mechanism on the enamel surface after the abrasion test and the effects of mill additives on enamel surfaces were investigated by means of SEM-EDS analysis.

Materials and Methods

The experimental flow chart of the study is shown in Fig. 1.

Enamel Slurry Preparation

An Akcoat commercial product (RTU CB2910) for wet application was used and was coated on grey cast iron. The frit used in this study is sodium borosilicate based. The frit oxide composition is given in Table 1. 300 g of frit was used for the production of the enamel

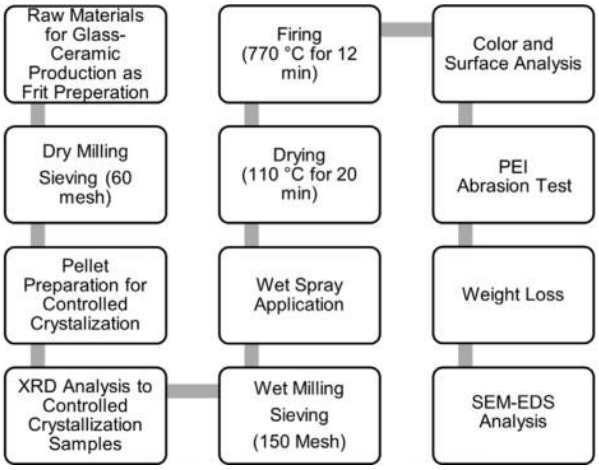

Fig. 1. Experimental Flow Chart.

Table 1. Composition of Studied Frit.

	Oxides	Composition (%)
RO_2	SiO_2, TiO_2, ZrO_2	57.52
R_2O	Na_2O, K_2O, Li_2O	13.26
RO	CaO, MgO, BaO, SrO, ZnO, NiO, CoO, CuO, MnO	13.57
R_2O_3	B_2O_3, Fe_2O_3, Al_2O_3, Cr_2O_3, Sb_2O_3	14.21
RO_3	MoO_3	0.16
R	F	1.21
R_2O_5	P_2O_5	0.07
	Total	100.0

Table 2. The amount of hard particles in each sample, with W0Q0 being the reference sample.

Hard Particles		
Sample	WC wt.%	Quartz wt.%
W0Q0	0	0
W0Q4	4	0
W0Q8	8	0
W4Q0	0	4
W8Q0	0	8
W4Q4	4	4
W8Q8	8	8

composition. The amount of mill additives was kept constant in all samples. 4 wt.% black pigment (Cr_2O_3-Fe_3O_4-CuO) was used as a colorant. As viscosity agents, 0.8 wt.% Amorphous silica (SiO_2), 4.5 wt.% caolinitic clay ($Al_2(OH)_4Si_2O_5$) and 0.3 wt.% sodium nitrite ($NaNO_2$) were used. Frits were dry milled by alumina-zircon balls for 15 min with 99.5% purity Tungsten Carbide (WC) (Global Tungsten, d_{90}=3 µm) and Quartz (SiO_2, coded as Q) (d_{90}=75 µm) additives with different mixture proportions, as presented in Table 2. The Alumina-zirconia mill balls weighed 850 g. Different ball sizes were used to obtain a more homogeneous milling. Ball diameter distribution was as follows: 15 mm, 20 mm and 25 mm with proportions of 33%, 33% and 34%, respectively. The dry milled batches were sieved through 60 mesh sieves.

Phase Analysis

Controlled crystallization (devitrification) was applied to the prepared batches to examine the crystallization behavior of the enamel. 15 g samples were taken from the dry batch and pressed with a cold press with 150 kN for 15 s. (Herzog HTP 40). Samples were fired for 12 min at 770 °C and cooled at room temperature. The cooling pellets were milled (Rocklabs Ring Mill) and XRD analyses were performed on pellet powders using Cu K_α radiation (Rigaku Miniflex 600).

Coating Application and Surface Analysis

The dry batches were wet milled to 100 g of enamel powder with 30 ml water for 90 s. Samples were sieved through 150 mesh sieves. Enamel slip was applied by spray method on gray cast iron plates (10×10×4.5 cm). Enamel-coated plates were dried at 110 °C for 20 min. The dried samples were fired in a box furnace at 770 °C for 12 min. CIE L*, a*, b* (color) values of enamel coated surfaces are measured by spectrophotometer (Konica Minolta CM-700d Spectrophotometer). In this system there are three different axes to define the color; L*, a* and b*. L* axis indicates the black/white or brightness of the color. Here, the color closest to black and white has the value 0 and 100 L*, respectively. The axes a* and b* determine the chromatic values of the color. The axis a* represents the redness (+) and greenness (-) of the color, while the axis b* represents the yellowness (+) and blueness (-) of the color. Sample surfaces were investigated by optical microscopy (Olympus SZ61) and by electron microscopy (Zeiss Supra 50VP SEM equipped with Oxford Instruments EDS). SEM images were obtained in the backscatter electron mode with an acceleration voltage of 20 kV and a working distance of 7.8-7.9 mm.

Abrasion Resistance Test

A PEI tester (Gabbrielli Technology Abrasimetro W3) according to ISO 10545-7 standards was used for determination of the abrasion resistance. The purpose of the test was to determine the abrasion resistance of the enamel plate by the rotation of the abrasive load on the surface. Within the scope of the test, the abrasive load mixture was placed on the enamel plate surface in a closed circle and the abrasives were rotated. The distribution of total load used within the scope of the test is as follows: 70.0 g of steel balls of diameter 5 mm; 52.5 g of steel balls of diameter 3 mm; 43.75 g of stell balls of diameter 2 mm; 8.75 g of steel balls of diameter 1 mm; 3.0 g of white fused aluminum oxide of grain size F80 according to ISO 8486 standards and 20 ml of distilled water. The total abrasive weight was 180 g. The rotation speed of the abrasive mixture was 300 rpm. The radius of the enamel coating area interacting with the abrasive mixture was 45 mm. The pre-weighed enamel-coated plates were subjected to a 5000 cycles abrasion test. The plates were dried at 110 °C for 30 min. Changes in weight loss for each sample were measured after the abrasion test.

Results and Discussions

XRD Results

XRD patterns of the enamel compositions are

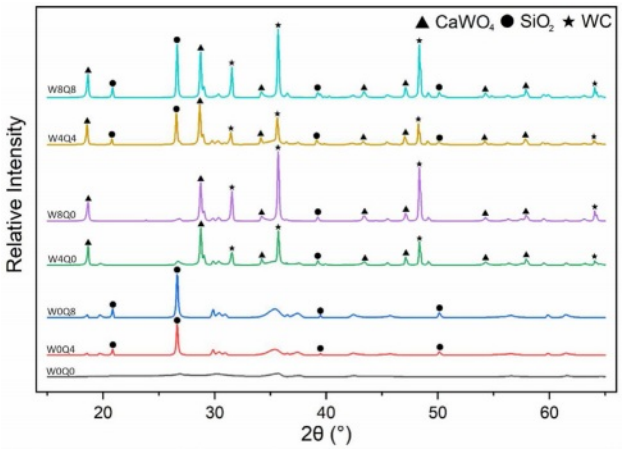

Fig. 2. Comparative XRD patterns of different enamel compositions.

presented in Fig. 2. Frits are amorphous due to their glassy structure. Frit and mill additives have a glass-ceramic structure as a result of controlled crystallization. Amorphous structure is seen in the XRD pattern of the standard sample, except for crystal peaks from pigments (Fig. 2:W0Q0). Samples W0Q4 and W0Q8 contain only 4 wt.% and 8 wt.% quartz, respectively. Adding quartz mill additive into the enamel recipe simply highlights the SiO_2 crystal peaks (#PDF:00-0078-1252). However, when WC was used as a mill additive, a new crystalline phase other than WC (#PDF:00-073-0471) was observed, namely $CaWO_4$ crystal ($CaWO_4$, #PDF:00-072-0257), which is a form of scheelite tungstates and consists of M^{2+} and $[WO_4]^{2-}$ ions [21, 22].

WC starts to oxidize at 500 °C. According to the reaction below, WC reacting with oxygen in different proportions converts to wolfram dioxide (WO_2) and WO_3 forms depending on the oxygen pressure in the system (Eq. 1-6) [23, 24]:

$$WC + O_2 \rightarrow WO_2 + C \quad (1)$$

$$WC + (3/2)O_2 \rightarrow WO_2 + CO \quad (2)$$

$$WC + (3/2)O_2 \rightarrow WO_3 + C \quad (3)$$

$$WC + 2O_2 \rightarrow WO_2 + CO_2 \quad (4)$$

$$WC + 2O_2 \rightarrow WO_3 + CO \quad (5)$$

$$WC + (5/2)O_2 \rightarrow WO_3 + CO_2 \quad (6)$$

Again, carbon dioxide (CO_2) and carbon monoxide (CO) gas formation is connected with oxygen pressure [23, 25-29]. A certain amount of WC added as a mill additive is oxidized during firing and it is converted to WO_3. In general, WO_3 can react with other oxides in the enamel composition. WO_3 reacts with CaO at 550 °C and forms the $CaWO_4$ compound (Eq. 7) [30-32].

$$WO_3 + CaO \rightarrow CaWO_4 \quad (7)$$

Also, sodium oxide (Na_2O) and potassium oxide (K_2O), which are other alkali metals present in the frit composition, do not react with WO_3, due to the low firing temperature (<770 °C) [33, 34]. WO_3 tends to react with alkaline earth metals (beryllium (Be), magnesium (Mg), calcium (Ca), strontium (Sr), barium (Ba) and radium (Ra)) [30, 35, 36]. The oxide forms of alkaline earth metals (MeO) are prone to react with WO_3 [30, 37].

$$MeO + WO_3 \rightarrow MeWO_4 \quad (8)$$

Theoretically, WO_3 can react with 4B and 6B elements. Yet, conditions such as firing temperature or oxygen base pressure are not suitable for these reactions to occur. Transition metal oxides Mo, Mn, Fe, Co, Ni, Cu and Zn are in the form of metal oxides (M_xO_y) in the enamel composition [38, 39]. Transition metal oxides (A) form the AWO_4 phase with wolfram oxides (Eq. 8) and these phases appear in the chloride or nitrate form [38, 39]. Nevertheless, due to the low amount of these transition metal oxides in the enamel composition, new crystals may not have formed or may not have been detected by XRD analysis.

Surface and Microstructure Analysis

The CIE L*, a*, b* values of enamel coatings applied on cast iron in SCE65 form are shown in Fig. 3. An increase in L* value is observed with the addition of mill additives Q and WC. The highest L* value is obtained when Q and WC are added to the enamel composition at the same time. The same amount of black pigment was used in all samples, but the pigment/enamel composition ratio decreases with the addition of Q and WC mill additives, so that the pigment's dyeability decreases

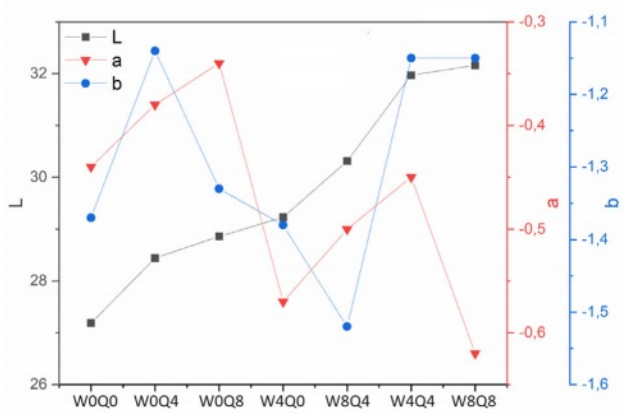

Fig. 3. CIE L*, a*, b* values of the samples.

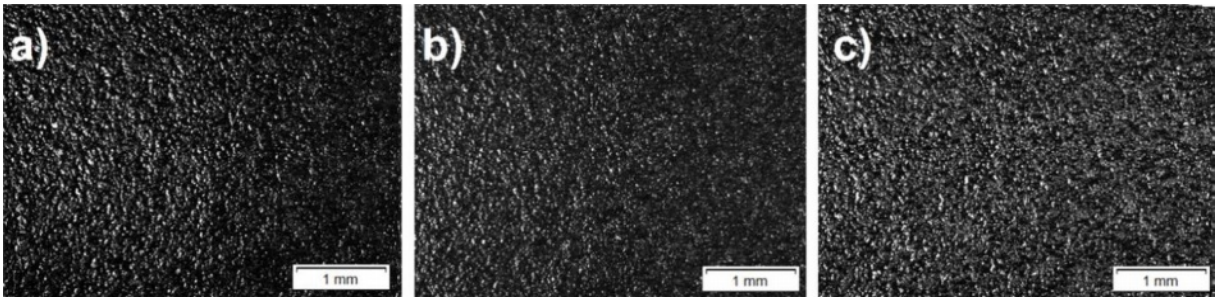

Fig. 4. Optical images of as-prepared only quartz-added sample surfaces a) W0Q0, b) W0Q4 and c) W0Q8.

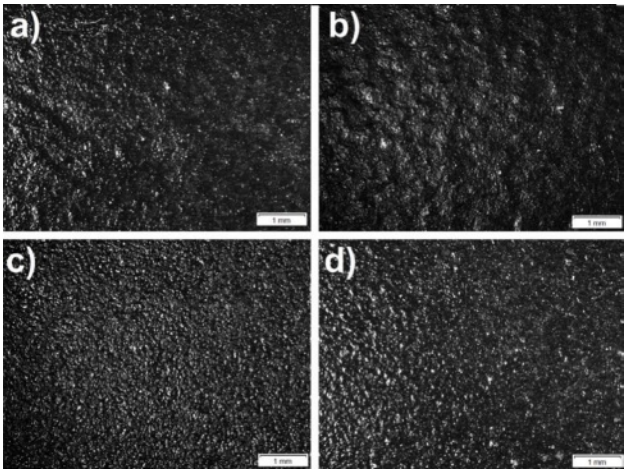

Fig. 5. Optical images of as-prepared sample surfaces a) W4Q0, b) W8Q0, c) W4Q4 and d) W8Q8.

and the coating surface becomes whiter. In addition, the a* and b* values are determined as –0.47±0.015 and –1.29±0.04, respectively. The standard deviations from the average values of a* and b* are acceptable.

Fig. 4 presents the optical images of the as-prepared reference sample and only Q-doped samples. Standard and Q added samples have an overall surface appearance of enamel coatings.

In Fig. 5 optical images of W4Q0, W8Q0, W4Q4 and W8Q8 sample surfaces are presented. The enamel coating prevents gases from forming due to high surface tension as well as preventing low fluidity from leaving the structure CO and CO_2 gases formed during the oxidation of WC cause closed porosities in the structure [40]. Bright and dark regions indicate apexes and dents, respectively. Unlike the samples with only WC additive, surface blisters are observed on the surfaces of the samples where two mill additives are added. The surfaces of W4Q4 and W8Q8 are similar to those of standard and SiO_2 added samples (Fig. 4c-5d).

Fig. 6 shows the SEM images of the as-prepared sample surfaces. SEM images were obtained in back-scattered electron (BSE) mode. The W0Q0 sample has a standard enamel appearance coated on gray cast iron. Open pores are visible on the sample surface (Fig. 6-a, Spot-1). The parts seen as white dots on the surface are Cr-Fe-Cu-based black pigments (Fig. 6-a, Spot-2). Quartz is the main network-former of glass matrix in vitreous enamel [1]. The addition of SiO_2 increases the glassy phase formation in the structure and causes a reduction of porosity (Fig. 6-b). Large pores (Fig. 6-c, Spot-1) and small pores (Fig. 6-c, Spot-3) are seen on the surface of the W8Q0. The volume of pigments on the surface decreases (Fig. 6-c, Spot-2). WC and $CaWO_4$ can be detected on the surface by EDS analysis (Fig. 6-c, Spot-4). The homogeneity of the enamel surface increases with the addition of SiO_2 (Fig. 6-d-W8Q8). According to EDS analysis, Spot 2 in Figs. 6-c and Fig. 6-d corresponds to a WC- and $CaWO_4$-rich region.

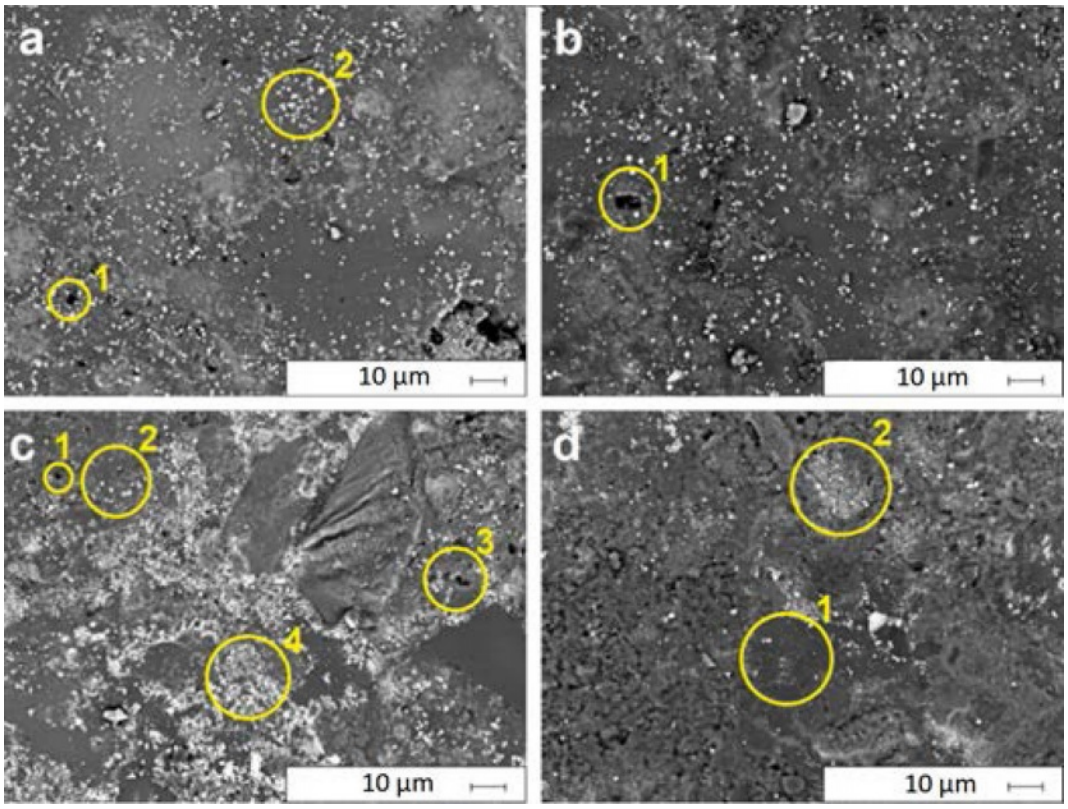

Fig. 6. SEM images before PEI abrasion tests a) W0Q0, b) W0Q8, c) W8Q0, and d) W8Q8.

The $CaWO_4$ distribution caused by WC oxidized on the surface decreases and the appearance of the glass-ceramic matrix increases (Fig. 5-d Spot-2).

Abrasion Resistance

The abrasion mechanisms of enamel coatings are examined in two different ways: on the surface and subsurface levels [15, 41]. The surface abrasion mechanism of enamel coatings develops with crack formation and nucleation at the grain boundaries. Subsurface abrasions, on the contrary, cause greater damage than on the surface abrasion [1, 15, 41]. There are two main strengthening mechanisms to improve the mechanical properties of vitreos enamel coating surfaces: frit modification and mill additive [1]. The most widely used mechanism to prevent or decrease crack formation is by adding a secondary phase to the grain boundaries. In this study, the improvement of the surface abrasion resistance of enamel was investigated. Weight loss method was chosen to measure the abrasion resistance of the enamel coating. The enamel coating with the lowest weight loss after the PEI abrasion test (according to ISO 10545-7) is defined as the optimum sample. PEI abrasion resistance test results are given in Fig. 7. According to the results of the PEI abrasion test, the sample with the lowest abrasion resistance is the W0Q0 sample, whose mass loss is 0.305 g. The incorporation of SiO_2 as a mill additive leads to an enhancement in abrasion resistance. While the weight loss of sample W0Q4 with 4 wt.% SiO_2 amounts to 0.275 g, the loss in the sample with 8 wt.% SiO_2 amounts to 0.152 g. WC addition to the enamel composition improves abrasion resistance more than the effect of SiO_2 addition. However, the 8 wt.% WC addition reduces abrasion resistance only slightly. Due to the hardness and mechanical strength of WC, it shows more resistance to mechanical abrasives than SiO_2. Weight loss in the W4Q0 sample containing 4 wt.% WC is 0.170 g. Weight loss increases to 0.203 g with the contribution of 8 wt.%. The mechanical effect of WC and SiO_2 against mechanical abrasives results in improved abrasion resistance. Weight loss is measured as 0.193 g in the W4Q4 sample with 4 wt.% WC and 4 wt.% SiO_2. With an increase in the Quartz rate, the oxidation of WC decreases, and the W8Q8 sample, containing 8 wt.% additives, yields the best abrasion resistance, with a weight loss of 0.147 g.

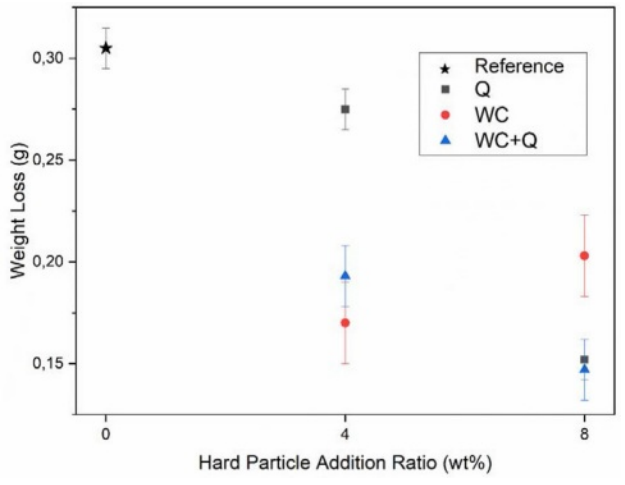

Fig. 7. Weight loss of samples after 5000 cycles PEI abrasion test.

Fig. 8 show back-scattered electron (BSE) images of the samples after the abrasion resistance test, respectively. Oxidation reactions and gas outlets that occur during firing lead to porosity on the surface (open pores (Spot-1 in Figs. 6-a and 6-b) or in the structure (bubble or closed pores (Fig. 8-a Spot-2)). Pore dimensions can be both in micro (Fig. 8-a Spot-3) and macro form (Fig. 8-a Spot-1). Pores increase crack nucleation and weaken the mechanical properties of enamel coatings [1, 17, 41]. In the W0Q0 sample's BSE images after the PEI test, brittle fracture is observed (Fig. 8-a). Cracks nucleate at grain boundaries. The glassy phase on the left side of the image was separated from the structure after abrasion and caused weight loss. The closed porosity formed in the structure becomes visible after the PEI test. Porosities lead to a decrease in abrasion resistance [11]. Small white dots on the BSE images are pigments (Fig. 8-b Spot-1). With the addition of SiO_2, the glassy phase increases and closed pore formation and dimensions decrease (Fig. 8-b Spot-2). Abrasion becomes homogeneous and cracks continue to nucleate at grain boundaries. (Fig. 8-b). The 4 wt.% SiO_2 additive is homogeneously distributed in the glassy phase (Fig. 8-b). SiO_2 addition reduces the expansion coefficients of enamels, thereby reducing thermal stress [42]. The reduction of thermal stress reduces crack formation during abrasion. SiO_2 crystals that resist mechanical abrasion improve abrasion resistance by preventing crack nucleation within the glassy structure [18]. An increase in the SiO_2 rate causes regression in homogeneous distribution (Fig. 8-c). However, with the increase of mechanical strength, the weight loss is reduced. The large white dots (Fig. 8-c Spot-1) seen on the surface are $CaWO_4$ crystal, while the gray areas seen on the glass structure have WC and $CaWO_4$ structures. Due to its high density during firing, WC crystals are most probably embedded in the glassy phase. $CaWO_4$, which is formed during oxidation, may slow the oxidation of WC and allow the additive to remain in a high hardness carbide form (Fig. 8-c). WC oxidized during firing increases the number and volume of closed porosity in the structure with the CO and CO_2 gases it generates. Closed porosities increase due to oxidation with an increasing WC amount. Due to the low mechanical strength of the porosity, abrasion causes high weight losses from the surface. As a result of the constant firing parameters, SiO_2 may absorb the temperature and the energy required to oxidize the WC and causes more WC to remain in the structure. It can be observed that crack nucleation decreases in the surface images after the PEI test (Fig. 8-d). WC prevents crack

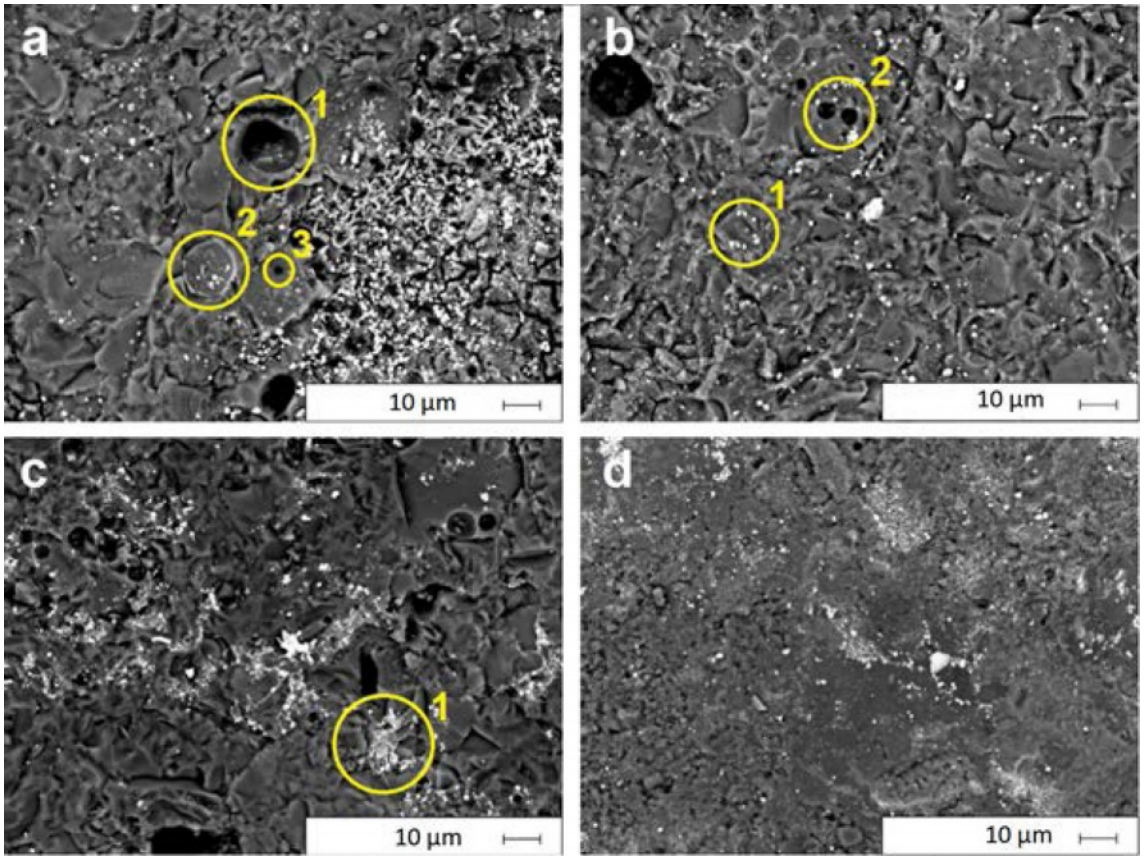

Fig. 8. SEM images of the abraded surfaces of the a) W0Q0, b) W0Q8, c) W8Q0, d) W8Q8 after PEI abrasion test.

nucleation by resisting the abrasive mechanical effects. The addition of high hardness spherical particles, such as WC, to the matrix ensures that the stress caused by mechanical abrasives is prevented without causing fracture [18]. In addition, the WC accumulated on the grain boundaries prevented the progress of the fracture by acting as a secondary phase. The slowing of the fractures had a decreasing effect on mass loss. With the decrease in oxidation, CO and CO_2 gas formation decreases. Therefore, pore formation is prevented and causes the surface to remain more homogeneous. In sample W4Q4, the high mechanical strengths of WC grains improve abrasion resistance. However, the surface remains rougher compared to W0Q4, which contains the same amount of SiO_2. With the addition rate increasing to 8 wt.%, porosity increases. Accordingly mechanical properties decrease.

Conclusions

The abrasion resistance effects of quartz (SiO_2) and wolfram carbide (WC) mill additives in enamel compositions were studied. According to the PEI abrasion test the standard sample weight lost was measured as 0.305 g. With 4 wt.% and 8 wt.% SiO_2 mill addition, an increase of 9.83% and 49% in the abrasion resistance was measured, respectively. WC addition of 4 wt.% (W4QO) to the structure positively affected the abrasion resistance, while the abrasion resistance decreased with the increase of the WC additive amount to 8 wt.% (W8QO). The abrasion resistance of the sample containing 4 wt.% WC improved by 44.26% compared to the standard sample (W0Q0). However, the sample containing 8 wt.% WC additive showed only 33.44% better abrasion resistance compared to the standard sample.

The samples containing WC-Quartz combination yielded the best results. The abrasion resistance of the sample containing 4 wt.% WC and 4 wt.% 0 Quartz (W4Q4) additive increased by 35.4%. The increase in abrasion resistance was measured as 51.8% in W8Q8 sample containing 8 wt.% WC and 8 wt.% Quartz. SiO_2 addition has increased the abrasion resistance of the coatings by reducing the thermal stress and preventing crack nucleation. This structure increased the compatibility of the hard particle within the structure. In the case of WC addition into the enamel composition, it was seen that WC oxidizes during firing to form wolfram oxide (WO_3). Subsequently, WO_3 combines with calcium oxide (CaO) from the frit to form a scheelite ($CaWO_4$) compound. The $CaWO_4$ phase served as a intermediate phase between the WC and the enamel glass phase.

It was demonstrated that the porosity of the enamel was related to the WC that oxidizes during firing to produce carbon monoxide (CO) and carbon dioxide (CO_2) gases.

With an increasing WC rate, oxidation increased and the porosity formation in the structure increased; hence, mechanical properties decreased. The non-oxidized WC crystals resisted abrasives and prevented crack nucleation in the glass-ceramic structure. Quartz addition slowed the oxidation of the WC, showing its refractory properties. It also increased the incorporation of the WC with the matrix due to network former properties.

References

1. A.I. Andrews, S. Pagliuca, and W.D. Faust, in "Porcelain (Vitreous) Enamels and Industrial Enamelling Processes. The Preparation, Application and Properties of Enamels" (The International Enamellers Institute, 2011).
2. G. Kaya, B. Karasu, and A. Cakir. J. Ceram. Process. Res. 12[2] (2011) 135-139.
3. L. Bragina, O. Shalygina, N. Kuryakin, V. Annenkov, N. Guzenko, K. Kupriyanenko, V. Hudyakov, and A. Landik, Powder electrostatic enamelling of household appliances, IOP Conf. Ser. Mater. Sci. Eng. 2[25] (2011) 012012.
4. W. Jiang, Y. Wang, and L. Gu, Mater. Lett. 62[2] (2008) 262-265.
5. D. Wang, Appl. Surf. Sci. 255[8] (2009) 4640-4645.
6. A. Zucchelli, G. Minak, and D. Ghelli, Strain. 46[5] (2010) 419-434.
7. A. Nikbakht, A.F. Arezoodar, M. Sadighi, A. Zucchelli, and A.T. Lari, Compos. Struct. 96 (2013) 484-501.
8. B.T. Garland, Mater. Des. 7[1] (1986) 44-48.
9. N.S.C. Millar and C. Wilson, in "Vitreous Enamel Coatings in Corrosion (Elsevier,1994) p.16:3-16:1.
10. J. Park, A. Öztürk, S. You, S. Park, W. Bae, and D. Shin, J. Ceram. Process. Res. 9[3] (2008) 230-233.
11. S. Rossi, C. Zanella, and R. Sommerhuber, Mater. Des. 55 (2014) 880-887.
12. A. Conde, J.J. de Damborenea, in"Reference Module in Materials Science and Materials Engineering" (Elsevier, 2016). p. 2330-2336.
13. G. McCombie and M. Biedermann, in "Encyclopedia of Food Chemistry" (Academic Press, 2019) p. 603-608.
14. K. Benzeşik, M. İpekçi, A. Yeşilçubuk, Ç. Şahin, and O. Yücel, in 19th International Metallurgical ve Materials Congress (IMMC), October 2018, edited by O. Yücel, H. Gür, G. Orhan, p. 437-440.
15. F.A. Petersen, J. Am. Ceram. Soc. 30[3] (1947) 94-104.
16. W.C. Spangenberg, J. Am. Ceram. Soc. 37[2] (1954) 48-52.
17. S. Rossi and E. Scrinzi, Chem. Eng. Process. Process. Intensif. 68 (2013) 74-80.
18. S. Rossi, N. Parziani, and C. Zanella, Wear. 332-333 (2015) 702-709.
19. L.Telmenbayar and J. Temuujin, J. Ceram. Process. Res. 17[5] (2016) 489-493.
20. S. Wang, Y. Xue, C. Ban, Y. Xue, A. Taleb, and Y. Jin, Surf. Coat. Tech. 385 (2020) 125390.
21. S. Kaowphong, T. Thongtem, and S. Thongtem, J. Ceram. Process. Res. 11[4] (2010) 432-436.
22. T. Thongtem, A. Phuruangrat, and S. Thongtem, J. Ceram. Process. Res. 9[3] (2008) 258-261.
23. A.E. Newkirk, J. Am. Chem. Soc. 77[17] (1955) 4521-4522.
24. H.A. Wriedt, Bull. Alloy. Phase Diagrams. 10[4] (1989) 368-384.
25. W.W. Webb, J.T. Norton, and C. Wagner, J. Electrochem. Soc. 103[2] (1956) 107.
26. V.B .Voitovich, V.V. Sverdel, R.F. Voitovich, and E.I. Golovko, Int. J. Refract. Met. Hard. Mater. 14[4] (1996) 289-295.
27. C.A. Ribeiro, W.R. De Souza, M.S. Crespi, J.A. Gomes Neto, and F.L. Fertonani, J. Therm. Anal. Calorim. 90[3] (2007) 801-805.
28. A.S. Kurlov and A.I. Gusev, Int. J. Refract. Met. Hard. Mater. 41 (2013) 300-307.
29. S.A. Humphry-Baker and W.E. Lee, Scr. Mater. 116 (2016) 67-70.
30. L.L.Y. Chang, M.G. Scroger, and B. Phillips, J. Am. Ceram. Soc. 49[7] (1966) 385-390.
31. A.M. Abdel-Rehim, J. Therm. Anal. Calorim. 64[3] (2001) 1283-1296.
32. J.C. Grivel and J. Phase, Equilibria. Diffus. 33[1] (2012) 46-50.
33. R.J.H. Gelsing, H.N. Stein, and J.M. Stevels, Recl. Des. Trav. Chim. Des. Pays-Bas. 84[11] (1965) 1452-1458.
34. Q. Wei, H. Shi, Xi. Cheng, L. Qin, G. Ren, and K. Shu, J. Cryst. Growth. 312[11] (2010) 1883-1885.
35. L.T. Aldrich, J. Appl. Phys. 22[9] (1951) 1168-1174.
36. G., Flor, R. Riccardi Sect. A. J. Phys. Sci. 31[6] (1976) 619-621.
37. Q. Guo and O.J. Kleppa, Thermochim. Acta. 288[1-2] (1996) 53-61.
38. J.T. Kloprogge, M.L. Weier, L.V. Duong, and R.L. Frost, Mater. Chem. Phys. 88[2–3] (2004) 438-443.
39. S. Dey, R.A. Ricciardo, H.L. Cuthbert, and P.M. Woodward, Inorg. Chem. 53[9] (2014) 4394-4399.
40. D. Song, R. Tang, F. Yang, Y. Qiao, J. Sun, J. Jiang, and A. Ma, Materials. 11[11] (2018) 2183.
41. S. Rossi and F. Russo, Encyclopedia. 1[2] (2020) 388-400.
42. S. Reis, M. Koenigstein, L. Fan, G. Chen, L. Pavic, and A. Moguš-Milankovic, Materials. 12[2] (2019) 248.